

# Hyperion: Hierarchical Scheduling for Parallel LLM Acceleration in Multi-tier Networks

Mulei Ma, *Graduate Student Member, IEEE*, Minrui Xu, *Member, IEEE*, Zihan Chen, *Member, IEEE*,  
Tony Q. S. Quek, *Fellow, IEEE*, and Yang Yang, *Fellow, IEEE*

**Abstract**—LLMs are increasingly executed in edge where limited GPU memory, and heterogeneous compute jointly constrain deployment and motivate model partitioning and request scheduling. In this setting, achieving low latency depends on both model placement and the scheduling of incoming requests across heterogeneous nodes. These two problems are tightly coupled, as a suboptimal scheduler can negate the benefits of a good partition, and vice versa. In this paper, we propose Hyperion, a hierarchical two-stage framework that jointly optimizes partitioning and scheduling to minimize end-to-end latency for pipelined LLM inference in multi-tier networks, balancing compute and memory across tiers while introducing negligible runtime overhead and requiring no model retraining. Motivated by the observation that partition choices evolve on slower timescales than request arrivals, Stage 1 performs offline, inter-tier partitioning via a Hyperion Split with Dynamic Programming (HypSplit-DP) procedure to produce balanced stage times under tier capacity and memory constraints; to adapt to time-varying load, Stage 2 performs online, intra-tier scheduling with a lightweight Hyperion Scheduling for Real-Time (HypSched-RT) algorithm that maps each request to the best available node using real-time estimates of queue length and effective capacity. Experimental results on multi-tier inference tasks demonstrate that Hyperion significantly reduces end-to-end latency by up to 52.1% and 31.2%, with the Phi-3-medium, compared to the GPipe and HEFT baselines, respectively. Furthermore, Hyperion shows superior scalability in long-sequence generation, maintaining a 44.5% lower latency and achieving higher GPU utilization.

**Index Terms**—Large Language Models (LLMs), Multi-tier Networks, Edge Computing, Hierarchical Scheduling

## I. INTRODUCTION

Large language models (LLMs) based on the Transformer architecture have achieved revolutionary breakthroughs in the field of natural language processing (NLP) [1]. The rise of LLMs is transforming cloud/data-center workloads and sparking strong interest at the edge [2]. According to a forecast by the International Data Corporation (IDC), by 2025, over 75% of data will be generated at the edge [3]. Rapid Internet of Things (IoT) and 5G development is driving strong demand for efficient on-device AI across smartphones, wearables, etc. In these scenarios, low latency and real time processing are crucial; deploying LLMs on edge devices can help provide more intelligent and personalized services [4].

However, edge devices still face severe limitations in computing and memory resources [5], making it challenging to run LLMs directly [6]. For example, NVIDIA Jetson Nano typically have memory ranging from 4 GB to 12 GB and computing capabilities around 472 gigaflops (GFLOPS), whereas

GPT-3 has a model size exceeding 350 GB and requires approximately 314 GFLOPS of computation per token during inference [7]. This limitation extends beyond single devices, rendering flat, single-tier networks similarly impractical for efficient LLM inference. A single-layer topology precludes proximity-aware, sensitivity-driven deployment of inference stages, resulting in poor load balancing and diminished fault tolerance. Therefore, adopting a multi-tier network architecture offers an effective path for deploying LLMs in resource-constrained Scenarios [8].

To support edge side LLM deployment, we adopt a multi-tier network architecture. As shown in Fig. 1, this integrated multi-tier design comprises devices distributed across three tiers under the central cloud [9]. Through Network AI Management and Orchestration (NAMO), the cloud coordinates cross-domain resources, and orchestrates task placement [10]; tier-level Network AI Logic and Control (NALC) modules execute real-time, region-local optimization. The multi-tier design also offers practical deployability, providing enhanced privacy and flexibility while aligning with geographic or organizational boundaries [11]. For example, in manufacturing, Tier 1 sits at each production line, Tier 2 spans the campus across multiple lines, and Tier 3 resides in the company’s headquarters, connected via secure wireless backhaul.

Despite the potential of this multi-tier architecture, efficiently deploying LLMs within such a framework faces two hurdles. First, the edge environment is characterized by device heterogeneity, with hardware ranging significantly in performance from high-performance edge servers and routers to low-power sensors [12]. Compounding this issue, statistics indicate that edge device idle rates can be as high as 60%, leading to systemic resource underutilization [13]. Second, there is a research gap in optimizing LLMs for these specific network structures. Current research primarily focuses on techniques like model compression, knowledge distillation, and model pruning to adapt to the resource constraints of edge devices [14]. Moreover, existing distributed deep learning strategies are poorly optimized to exploit resources across heterogeneous, multi-tier computing networks, leading to low system efficiency [15]. Most existing scheduling algorithms fail to consider the specific topology characteristics of multi-tier networks, leaving a gap in cross-tier optimization [16].

Bridging this research gap is complex, as optimizing inference performance in such multi-tier architectures hinges on two tightly coupled decisions. The first is inter-tier model partitioning: segmenting the model across heterogeneous tiers to enable pipeline parallelism. The second is intra-tier task

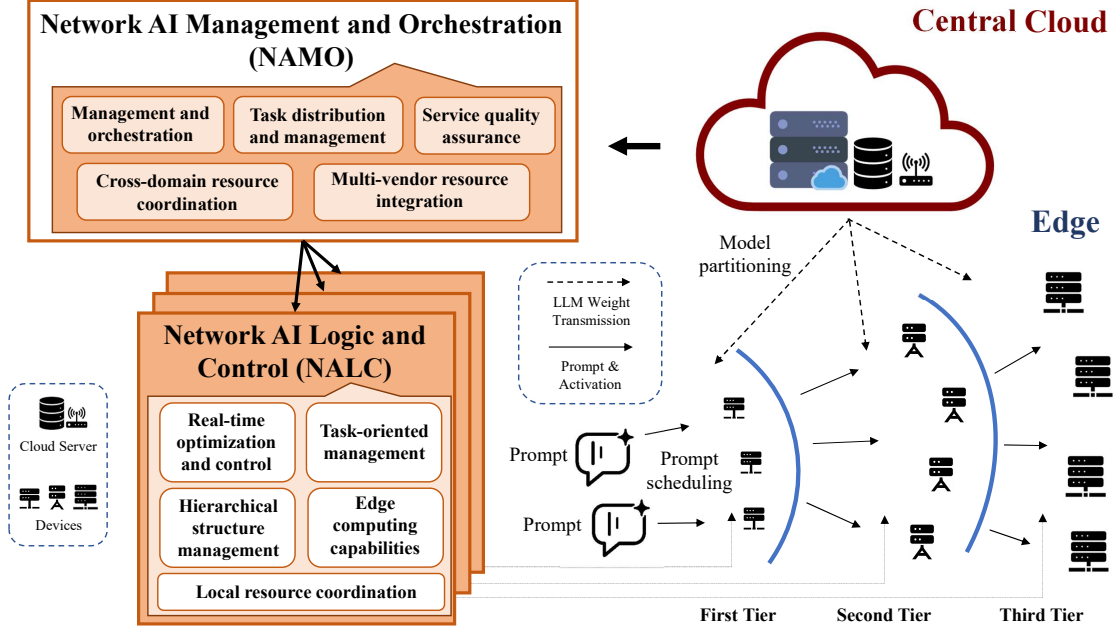


Fig. 1: Multi-tier Network Architecture Incorporating three Edge Tiers for Optimized LLM Inference and Resource Management

scheduling: dispatching incoming requests to the most suitable nodes within a tier under resource constraints. Partitioning determines compute and communication balance, while scheduling governs queueing delay and resource contention. Optimizing them in isolation yields imbalanced pipelines and head-of-line blocking that dominate end-to-end latency [17].

Therefore, to achieve efficient inference across multi-tier networks, we propose Hyperion, a framework that introduces a two-stage strategy. Crucially, our work moves beyond the isolated, single-tier scheduling common in current research by creating a unified, holistic optimization strategy that considers the entire network hierarchy. To this end, we first formulate a comprehensive Min-Max problem aimed at minimizing the inference latency, denoted as  $(\mathcal{P}_0)$ , and then introduce Hierarchical Parallel Execution and resource-aware scheduling for LLM Inference on multi-tier Networks (Hyperion), which decouples the complex joint optimization problem into two less complex, sequential sub-problems. First Stage: Model Partitioning and inter-tier Allocation Strategy  $(\mathcal{P}_1)$ , which is an offline static process that partitions the LLM's blocks across tiers. By considering each tier's computing and memory resources to optimize load balancing, this stage leverages a Hyperion Split with Dynamic Programming (HypSplit-DP) algorithm to determine the optimal partition strategy. Second Stage: intra-tier Task Scheduling Strategy  $(\mathcal{P}_2)$ . Taking the fixed partition from first stage as a given, this stage leverages the Hyperion Scheduling for Real-Time (HypSched-RT) algorithm, which achieves optimal  $O(K_j)$  time complexity via a single linear scan, performing online scheduling of prompts/activations to identify the most suitable intra-layer nodes for pipeline paral-

lel. This hierarchical decoupling strategy significantly reduces the overall computing complexity, providing a scalable and efficient solution. The main contributions of this study are summarized as follows:

- 1) We formulate the inference latency challenge in heterogeneous, memory-constrained multi-tier networks as a Min-Max orchestration problem  $(\mathcal{P}_0)$ . We propose Hyperion, a framework that pioneers a dual-driven (model & task aware), two-stage strategy, decoupling offline model partitioning  $(\mathcal{P}_1)$  from online task scheduling  $(\mathcal{P}_2)$  to achieve holistic optimization.
- 2) For the offline stage, we design a HypSplit-DP algorithm that delivers a provably optimal, resource-aware partitioning of the LLM's blocks across heterogeneous tiers by balancing computing and memory constraints.
- 3) For the online stage, we introduce the lightweight HypSched-RT approach, which dynamically assigns incoming inference requests to the optimal node within each tier by considering real-time device status and availability, guaranteeing a stable performance upper bound with an linear  $O(K_j)$  complexity and negligible runtime overhead.
- 4) We evaluate the Hyperion framework through extensive experiments. Results demonstrate Hyperion's performance, reducing end-to-end latency by up to 31.2% against the HEFT baseline and 52.1% against GPIPE (specifically 44.5% in long-sequence generation), validating its efficiency and scalability.

The remainder of this paper is organized as follows. Section II reviews prior work in distributed LLM inference and

resource scheduling. Section III details our system model and the optimization problem formulation. Section IV introduces the Hyperion framework, detailing its two-stage scheduling algorithms. Section V provides an extensive experimental evaluation against several baselines. Finally, Section VI we conclude the paper.

## II. RELATED WORK

In recent years, as LLMs have continued to grow in scale, efficiently deploying and inferring LLMs in resource constrained edge scenarios has become an important research area [18]. This paper focuses on the following four aspects of related work: distributed accelerated inference of LLMs in edge, resource scheduling, parallel computing (pipeline parallelism, tensor parallelism, etc.), and the scheduling of LLMs in multi-tier computing networks [19].

### A. Distributed Accelerated Inference of LLMs in Edge Computing

In edge scenarios, the computing and memory resources of devices are limited, making it difficult to directly deploy LLMs [20]. To address this issue, researchers have proposed various distributed inference acceleration methods. Teerapittayanan et al. [21] introduced the concept of Distributed Deep Neural Networks (DDNN), which partitions the model into multiple segments that are executed across the cloud, edge, and end devices, reducing latency and bandwidth consumption. This work demonstrated that collaborative execution across different tiers significantly reduces inference time. To reduce computing load, BranchyNet [22] introduced an early exit mechanism that allows the model to output results early when accuracy requirements are met. F. Dong et al. [23] further proposed Adaptive Early Exit, which dynamically adjusts early exit points to improve inference efficiency on edge devices. Model compression are widely used on edge devices. Han et al. [24] proposed Deep Compression, which uses pruning, quantization, and Huffman coding to reduce model size by 35 times and computing load by 49 times. Li et al. [25] designed a lightweight model architecture for Transformer models to enable efficient inference on mobile devices. Hinton et al. [26] introduced Knowledge Distillation, where a smaller model learns to mimic the behavior of a larger model, achieving model simplification. Kim et al. [27] applied knowledge distillation to Transformer models, significantly improving the performance of smaller models. However, these methods still face limitations when dealing with LLMs that have over tens of billions of parameters. Achieving efficient distributed inference for LLMs in edge computing while maintaining model performance remains a challenge.

### B. Resource Scheduling for LLMs in Edge Computing

Efficient resource scheduling is a hotspot in LLM deployment research. Wang et al. [28] proposed a deep reinforcement learning based computation offloading strategy that dynamically allocates resources in multi user and multi task edge environments. Their model considers factors such

as communication delay, energy consumption, and device resources to minimize task completion time. Gu et al. [29] designed a collaborative computing framework that allows multiple edge devices to jointly execute tasks. By decomposing and scheduling tasks, they significantly improved system throughput and resource utilization. Lin et al. [30] proposed a joint optimization strategy for task offloading and resource allocation using game theory for multi device collaboration. In edge environments, device heterogeneity poses a challenge for resource scheduling. Xiao et al. [31] introduced a resource management framework for heterogeneous edge environments that considers device computing capacity, energy consumption, and reliability to achieve efficient LLM deployment. During the process of computation offloading, data security and privacy protection are also crucial. Zhou et al. [32] proposed a secure computation offloading framework that uses differential privacy and encryption techniques to safeguard user data security. While these methods provide a foundational basis, the device heterogeneity and fragmented resources inherent in multi-tier networks pose distinct challenges. An effective resource scheduling strategy is thus critical for the optimal allocation of LLM partitions, which is a central aspect of our work.

### C. Parallel Computing of LLMs in Edge Computing

Parallel computation play a vital role in accelerating the training and inference of LLMs. Huang et al. [33] proposed GPipe, which uses pipeline parallelism to assign different tiers of a model to different devices, significantly improving training efficiency. Goyal et al.'s PipeDream framework [34] further optimized the communication overhead of pipeline parallelism, achieving efficient training in heterogeneous environments. In edge computing, these methods can enable collaborative inference by mapping model blocks onto different edge devices. Megatron-LM [35] utilizes tensor parallelism to split large model parameters across multiple GPUs, enabling efficient model training. In edge environments, Laskaridis et al. [36] proposed the SPINN framework, which uses tensor parallelism to distribute model parameters across multiple edge devices, thereby enhancing inference performance. Narayanan et al. [37] introduced Pipeline Model Parallelism, combining data parallelism, model parallelism, and pipeline parallelism to achieve better scalability. In edge scenarios, this hybrid strategy can flexibly select parallel methods based on device resources and network conditions, enhancing overall system performance. In edge environments, network bandwidth and communication latency are bottlenecks for parallel computing. Shi et al. [38] proposed a communication-aware parallel training method that reduces communication overhead using techniques such as compression and pruning. Zheng et al. [39] designed an efficient parameter synchronization mechanism that reduces communication costs in distributed training. However, despite these advances, applying these techniques in edge requires overcoming challenges such as device heterogeneity and network limitations. Also, these methods primarily focus on single-tier optimizations and often overlook the unique topological characteristics of multi-tier networks,

leaving a research gap in holistic, cross tier scheduling. Our work addresses this by proposing a hierarchical framework that cohesively optimizes LLM deployment across the entire network hierarchy, accounting for its structural properties to enhance overall system efficiency.

#### D. Research on LLMs Scheduling in Multi-tier Computing Networks

Multi-tier Computing Networks integrate cloud, edge, and end devices, providing abundant and heterogeneous computing resources, thus bringing new opportunities and challenges for deploying LLMs. Li et al. [40] proposed CoEdge, which distributes different layers of LLMs across cloud, edge, and end devices, achieving hierarchical collaborative computing. Their experiments showed that this method reduces latency by 30% while maintaining model accuracy. Zhou et al. [41] designed a dynamic task decomposition and scheduling framework that dynamically adjusts task partitioning and scheduling strategies of LLMs based on real time network and device conditions. By predicting task execution time and communication delays, system performance optimization is achieved. Cen and Zhu [42] proposed NP-LLM, a unified framework that leverages large language models for 6G network-layer planning. This approach utilizes LLM generality to conduct scalable traffic optimization and resource allocation. Wang et al. [43] introduced a joint optimization scheduling strategy that simultaneously considers computing resources, communication resources, and energy consumption. Using multi objective optimization algorithms, they achieved a balance between system performance and energy efficiency. To address the challenges of high communication overhead for LLM serving in multi-tier networks, Wu et al. [44] proposed RecServe, a recursive offloading framework that employs hierarchical confidence evaluation and dynamic threshold adjustments. Their experiments demonstrated that RecServe enhances service quality and communication efficiency. Although extensive research has been conducted at different levels on LLM deployment and scheduling in edge and multi-tier computing networks, a comprehensive optimization approach that simultaneously considers model partitioning, resource scheduling, and task scheduling is still lacking. This study aims to fill this gap by proposing a two-stage task scheduling strategy to achieve efficient deployment of LLMs in multi-tier computing networks.

### III. SYSTEM MODEL AND PROBLEM FORMULATION

#### A. Modeling of LLM Structure

The inference process of the decoder only based LLMs can be represented as a linear Directed Acyclic Graph (DAG). As shown in Fig. 2, we use the Llama 3 as an example to illustrate the structure between these decoder blocks. Here, the attention mechanism is implemented as Grouped Query Attention (GQA), which incorporates Rotary Positional Encoding (RoPE). The Feed Forward Network utilizes a SwiGLU gating mechanism, and Root Mean Square Normalization (RMS Norm) is applied before both the attention and feed forward sub layers. These sub layers are sequentially arranged to form a decoder transformer block, and the overall LLM is

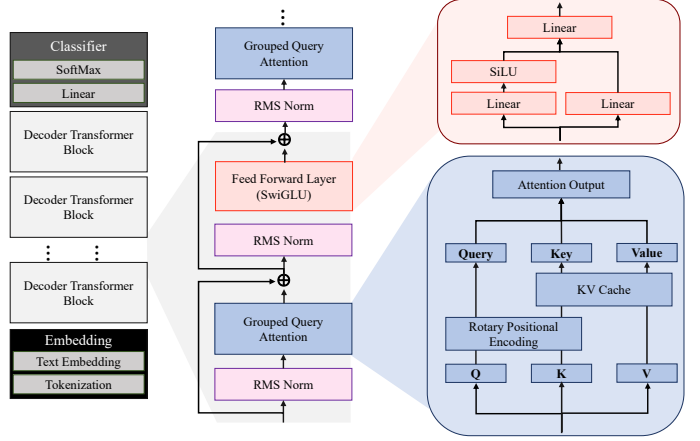


Fig. 2: Hierarchical Architecture of a Llama 3, from Decoder Blocks to Detailed GQA and SwiGLU Component Views.

constructed by stacking a series of these blocks. Despite this intricate internal structure, we maintain the abstraction of the entire decoder block as a single, atomic computing unit.

We abstract an LLM  $\mathcal{M}$  as a computation graph composed of  $N$  sequential decoder blocks. Let  $\mathcal{B} = \{B_1, B_2, \dots, B_N\}$  be the ordered set of decoder blocks that constitute the model, where  $N \in \mathbb{N}^+$  denotes the depth of the model. During the inference process, a strict sequential dependency exists among these blocks, which can be formally expressed as:

$$\forall i \in \{1, 2, \dots, N-1\}, \quad B_i \rightarrow B_{i+1}. \quad (1)$$

This implies that the output of block  $B_i$  serves as the exclusive input to block  $B_{i+1}$ . The execution of each decoder block  $B_i$  is accompanied by quantifiable computing and memory resource requirements. We define the following two functions to characterize its resource:

- *Computing Workload*: We define a function  $f : \mathcal{B} \rightarrow \mathbb{R}^+$ , where  $f(B_i) = f_i$  denotes the total number of Floating Point Operations (FLOPs) required to perform a single forward propagation of module  $B_i$ .
- *Memory Requirements*: We define a function  $m : \mathcal{B} \rightarrow \mathbb{R}^+$ , where  $m(B_i) = m_i$  denotes the memory space, measured in Gigabytes (GB), required on a computing node to load the weight parameters of module  $B_i$  and store its intermediate activation values during the forward propagation process.

We aggregate the computing workload and memory requirements of the entire model into  $N$ -dimensional column vectors, respectively:

$$\mathbf{f} = [f_1, f_2, \dots, f_N]^T \in \mathbb{R}^{N \times 1}. \quad (2)$$

$$\mathbf{m} = [m_1, m_2, \dots, m_N]^T \in \mathbb{R}^{N \times 1}. \quad (3)$$

### B. Multi-tier Heterogeneous Network Architecture

We consider a multi-tier network composed of  $T$  tiers, designed to host the pipelined inference tasks of a LLM. Let  $\mathcal{T} = \{1, 2, \dots, T\}$  be the index set of the network tiers. Each tier  $j \in \mathcal{T}$  consists of a cluster containing  $K_j$  nodes. We represent the set of nodes in tier  $j$  as  $\mathcal{K}_j = \{1, 2, \dots, K_j\}$ , where  $K_j = |\mathcal{K}_j|$  is the cardinality of nodes in that tier. The set of all nodes across the entire network can thus be expressed as  $\mathcal{K} = \bigcup_{j \in \mathcal{T}} \{(j, k) \mid k \in \mathcal{K}_j\}$ .

Each node  $(j, k)$  in the network (the  $k$ -th node within tier  $j$ ) is equipped with independent computing and memory resources. In this work, device heterogeneity is inter-tier. That is, within any given tier  $j$ , all nodes have the same hardware specification and are treated as homogeneous. The processing speed of a node is defined by its computing capacity, denoted as  $C_{j,k}$  and measured in FLOPs/s (Floating Point Operations per second). Correspondingly, the available memory size of a node is defined by its memory capacity,  $M_{j,k}$ , measured in GB. For the purpose of making model partitioning decisions, we need a metric to assess the overall service potential of each tier. To this end, we define the “effective capacity” of a tier, based on the optimal performance achievable within that tier, represented by the resources of its most capable node:

$$C_j^{\text{eff}} \triangleq \max_{k \in \mathcal{K}_j} \{C_{j,k}\}, \quad \forall j \in \mathcal{T}, \quad (4)$$

$$M_j^{\text{eff}} \triangleq \max_{k \in \mathcal{K}_j} \{M_{j,k}\}, \quad \forall j \in \mathcal{T}. \quad (5)$$

Here,  $C_j^{\text{eff}}$  and  $M_j^{\text{eff}}$  represent the effective computing capacity and effective memory capacity of a tier, respectively. This definition characterizes the performance upper bound that each tier can achieve under ideal scheduling conditions. When different parts of the model are deployed across various tiers, the transmission of intermediate data introduces communication latency.

We define an inter-tier communication latency, denoted as  $\tau_{j,l}$ , to be the time required to transmit an activation tensor from any node in tier  $j$  to any node in tier  $l$ . Given the linear pipeline structure of the model, the primary communication overhead occurs between adjacent tiers, we have  $\tau_{j,j+1} = S_{\text{act}}/R_{j,j+1}$ . Where,  $S_{\text{act}}$  is the size of the activation tensor and  $R_{j,j+1}$  is the achievable data rate. This data rate can be expressed as  $R_{j,j+1} = B_{j,j+1} \log_2(1 + \text{SINR}_{j,j+1})$ , where  $B_{j,j+1}$  is the allocated channel bandwidth, and  $\text{SINR}_{j,j+1}$  is the Signal-to-Interference-plus-Noise Ratio at the receiving node [45].

### C. Overall Optimization Problem

As illustrated in Fig. 3, we define the core challenge as an overall optimization Min-Max problem, denoted as  $\mathcal{P}_0$ . The figure outlines how this primary problem is decoupled into two manageable sub-problems: inter-tier Model Partitioning ( $\mathcal{P}_1$ ) and intra-tier Task Scheduling ( $\mathcal{P}_2$ ). The objective is to minimize the end-to-end latency for inference, which comprises two primary components: computing latency and communication latency.

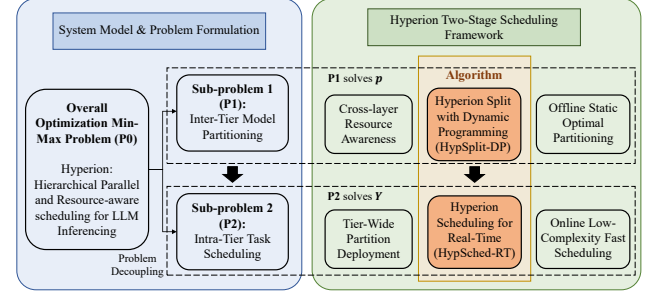


Fig. 3: Framework for Problem Decomposition in Hyperion, Detailing how the Overall Optimization Problem ( $\mathcal{P}_0$ ) is Decoupled into two Sub-problems, Inter-tier Partitioning ( $\mathcal{P}_1$ ) and Intra-tier Scheduling ( $\mathcal{P}_2$ ), and Solved Respectively.

To precisely formulate the model partitioning and task scheduling problems, we define two sets of decision variables. We employ a partitioning vector  $\mathbf{p} = (p_1, p_2, \dots, p_{T-1}) \in \mathbb{N}^{T-1}$  to define the partitioning scheme of the model. Herein,  $p_j$  denotes the global index of the last decoder block allocated to the  $j$ -th tier. For convenience, we introduce the auxiliary variables  $p_0 \triangleq 0$  and  $p_T \triangleq N$ . Consequently, the index set of the decoder blocks assigned to tier  $j \in \mathcal{T}$  can be expressed as:

$$\mathcal{I}_j(\mathbf{p}) = \{i \in \mathbb{N} \mid p_{j-1} < i \leq p_j\}. \quad (6)$$

We define a set of binary variables  $\mathbf{Y} = \{y_{j,k} \mid j \in \mathcal{T}, k \in \mathcal{K}_j\}$  to represent the task scheduling decisions. These variables are defined as follows:

$$y_{j,k} = \begin{cases} 1, & \text{task of tier } j \text{ scheduled to node } k, \\ 0, & \text{otherwise.} \end{cases} \quad (7)$$

The total latency, denoted as  $L_{\text{total}}(\mathbf{p}, \mathbf{Y})$ , is composed of the computing latency  $L_{\text{comp}}(\mathbf{p}, \mathbf{Y})$  and the communication latency  $L_{\text{comm}}(\mathbf{p})$ . For a given partitioning scheme  $\mathbf{p}$ , the computing workload assigned to tier  $j$  is defined as  $W_j(\mathbf{p}) = \sum_{i \in \mathcal{I}_j(\mathbf{p})} f_i$ . Should this workload be executed on a specific node  $(j, k)$ , the computation time would be  $W_j(\mathbf{p})/C_{j,k}$ . Consequently, factoring in the scheduling decision matrix  $\mathbf{Y}$ , the actual computation time for tier  $j$  is expressed as  $\sum_{k \in \mathcal{K}_j} y_{j,k} \frac{W_j(\mathbf{p})}{C_{j,k}}$ . Given that the tiers operate in a pipeline fashion, the overall computing latency is dictated by the performance of the slowest stage (i.e., the bottleneck). Therefore:

$$L_{\text{comp}}(\mathbf{p}, \mathbf{Y}) = \max_{j \in \mathcal{T}} \left\{ \sum_{k \in \mathcal{K}_j} y_{j,k} \frac{\sum_{i=p_{j-1}+1}^{p_j} f_i}{C_{j,k}} \right\}. \quad (8)$$

The total communication latency is the cumulative sum of the communication latency between all adjacent pipeline stages.

$$L_{\text{comm}}(\mathbf{p}) = \sum_{j=1}^{T-1} \tau_{j,j+1}. \quad (9)$$

Our goal is to minimize the total latency, which is the sum of communication and computing latency, denoted as  $\mathcal{P}_0$ :

$$\mathcal{P}_0 : \min_{\mathbf{p}, \mathbf{Y}} \left( \max_{j \in \mathcal{T}} \left\{ \sum_{k \in \mathcal{K}_j} y_{j,k} \frac{\sum_{i=p_{j-1}+1}^{p_j} f_i}{C_{j,k}} \right\} + \sum_{j=1}^{T-1} \tau_{j,j+1} \right), \quad (10a)$$

$$\text{s.t.} \quad 1 \leq p_1 < p_2 < \dots < p_{T-1} < N, \quad (10b)$$

$$\sum_{k \in \mathcal{K}_j} y_{j,k} = 1, \forall j \in \mathcal{T}, \quad (10c)$$

$$\sum_{i=p_{j-1}+1}^{p_j} m_i \leq \sum_{k \in \mathcal{K}_j} y_{j,k} M_{j,k}, \forall j \in \mathcal{T}, \quad (10d)$$

$$p_j \in \{1, 2, \dots, N-1\}, \forall j \in \mathcal{T}, \quad (10e)$$

$$y_{j,k} \in \{0, 1\}, \forall j \in \mathcal{T}, \forall k \in \mathcal{K}_j. \quad (10f)$$

The core objective of  $\mathcal{P}_0$  is to minimize the end-to-end total inference latency, which is formulated as the sum of two components. The first term in Eq. (10a) is the computing latency, which corresponds to the computation time of the longest running stage (i.e., the bottleneck) among all tiers. The second term in Eq. (10a) is the communication latency, defined as the aggregate time for transmitting intermediate activations between all adjacent tiers. This optimization problem is subject to a series of constraints. Constraint Eq. (10b) ensures the validity of the model partition vector  $\mathbf{p}$ , mandating that the partition must be strictly increasing and fall within a valid range, thereby partitioning the  $N$  decoder blocks into  $T$  non empty and contiguous subsequences. Constraint Eq. (10c) is the scheduling uniqueness constraint, which dictates that for each tier  $j$ , its task must be assigned to one and only one node within its node cluster  $\mathcal{K}_j$ . Constraint Eq. (10d) is the memory capacity constraint, which requires that the total memory footprint of all modules assigned to any given tier  $j$  must not exceed the available memory capacity  $M_{j,k}$  of the specific node selected by the scheduling decision  $y_{j,k}$ . Constraints Eq. (10e) and Eq. (10f) define the domains of the decision variables, specifying that the partition points  $p_j$  are integers, while the scheduling decisions  $y_{j,k}$  are binary variables.

#### D. Problem Decoupling and Hierarchical Solution

The overall optimization problem,  $\mathcal{P}_0$ , as previously formulated, is a Mixed Integer Nonlinear Programming (MINLP) problem [46]. Its decision variables include integer types (the model partition points  $\mathbf{p}$ ) and binary types (the task scheduling decisions  $\mathbf{Y}$ ), and its objective function contains a nonlinear max operator. Such problems are typically NP hard, and the computing complexity of solving them directly grows dramatically with the model depth  $N$  and the number of network nodes, making direct solutions difficult to apply.

To address this complexity, we propose a hierarchical framework that decouples the problem into two more tractable sub-problems. This two-stage approach serves as a heuristic

strategy designed to find an efficient solution. We leverage the difference in the time scales of the decisions to decouple the problem: model partitioning is generally a static, one time offline decision, whereas task scheduling is a dynamic, online decision that requires real time responsiveness. Based on this, we decouple  $\mathcal{P}_0$  into the following two sub-problems:

- *Sub problem 1: Cross Hierarchy Model Partitioning ( $\mathcal{P}_1$ )*:

This is a inter-tier, static planning problem. Its objective is to find the globally optimal model partition point vector  $\mathbf{p}$ , under the assumption that each hierarchy can find the optimal node.

- *Sub problem 2: Intra Hierarchy Task Scheduling ( $\mathcal{P}_2$ )*:

This is a intra-tier, dynamic decision problem. Given a fixed model partitioning scheme, when the input data for an inference request (i.e., the tokenized prompt for Tier 1, or intermediate activations for subsequent tiers) arrives at a specific hierarchy, an optimal execution node must be selected to execute the corresponding computational task based on the real time status of all nodes within that hierarchy.

The core of  $\mathcal{P}_1$  is to determine the optimal model partition vector, denoted as  $\mathbf{p}^*$ . To render the partitioning decision independent of the dynamic and instantaneous states of the nodes, we introduce a key assumption. When making the macroscopic partitioning decision, we replace the node level computing capability  $C_{j,k}$  and memory capacity  $M_{j,k}$  in the original problem with the tier level effective computing capability  $C_j^{\text{eff}}$  and tier level effective memory capacity  $M_j^{\text{eff}}$ , respectively. Consequently, the original objective function and its associated constraints are simplified, transforming it into an integer programming problem,  $\mathcal{P}_1$ , that depends solely on the partition variable  $\mathbf{p}$ .

$$\mathcal{P}_1 : \min_{\mathbf{p}} \left( \max_{j \in \mathcal{T}} \left\{ \frac{\sum_{i=p_{j-1}+1}^{p_j} f_i}{C_j^{\text{eff}}} \right\} + \sum_{j=1}^{T-1} \tau_{j,j+1} \right), \quad (11a)$$

$$\text{s.t.} \quad 1 \leq p_1 < p_2 < \dots < p_{T-1} < N, \quad (11b)$$

$$\sum_{i=p_{j-1}+1}^{p_j} m_i \leq M_j^{\text{eff}}, \forall j \in \mathcal{T}, \quad (11c)$$

$$p_j \in \{1, 2, \dots, N-1\}, \forall j \in \{1, \dots, T-1\}. \quad (11d)$$

$\mathcal{P}_1$  is to minimize the total system latency based on the estimated optimal performance of each tier. Constraints (Eq.(11b)) and (Eq.(11c)) ensure the validity of the partition, while constraint (Eq.(11d)) guarantees that the total memory required for the model chunks assigned to any tier does not exceed its effective memory capacity.

After obtaining the optimal partition  $\mathbf{p}^*$ , which is computed offline, the task for each tier  $j$  is determined. The subproblem  $\mathcal{P}_2$  is an online scheduling problem. When the intermediate activations for an inference task arrive at tier  $j$  from tier  $j-1$  (let the arrival time be  $t$ ), the intra-tier scheduler must select an execution node for it. This decision corresponds to determining the scheduling vector for tier  $j$ , denoted as  $\mathbf{Y}_j = \{y_{j,k}\}_{k \in \mathcal{K}_j}$ ,

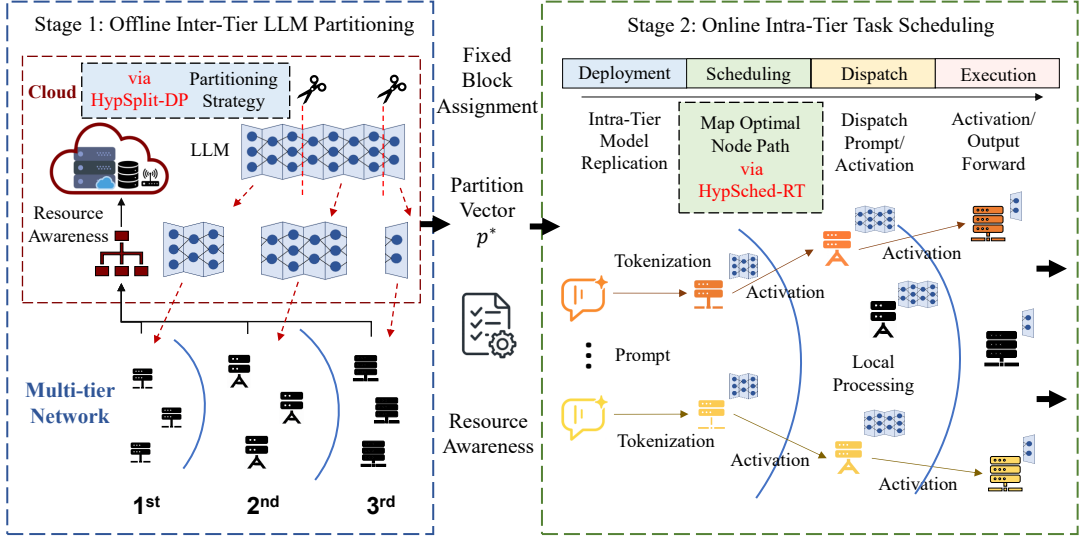


Fig. 4: System Architecture and Operational Workflow of the Hyperion Framework, Illustrating the end-to-end Process from Offline LLM Partitioning in the Cloud to Online, Real Time Task Execution Across the Multi-tier Network.

which is a component of the overall decision matrix  $Y$  defined in  $\mathcal{P}_0$ .

Unlike the offline static partitioning problem  $\mathcal{P}_1$ ,  $\mathcal{P}_2$  is a dynamic online decision that must be made in real time as tasks arrive. A high complexity scheduling algorithm would introduce scheduling overhead, creating a new latency bottleneck that would undermine the optimization goals. Therefore, the algorithm used to solve  $\mathcal{P}_2$  (i.e., HypSched-RT) must be lightweight and low complexity to ensure minimal overhead and meet these real time requirements.

The optimization objective here is to minimize the task's completion time at the current tier, which is composed of the node's queuing latency and the task's actual execution time. Let  $Q_{j,k}(t)$  be the task queue of node  $(j, k)$  at time  $t$ , and let  $T_{j,k}^{wait}(t)$  be the expected waiting time to process all tasks currently in that queue.

$$\mathcal{P}_2 : \min_{Y_j} \sum_{k \in \mathcal{K}_j} y_{j,k} \left( T_{j,k}^{wait}(t) + \frac{\sum_{i=p_{j-1}^*+1}^{p_j^*} f_i}{C_{j,k}} \right), \quad (12a)$$

$$\text{s.t. } \sum_{k \in \mathcal{K}_j} y_{j,k} = 1, \quad y_{j,k} \in \{0, 1\}, \quad (12b)$$

$$\sum_{i=p_{j-1}^*+1}^{p_j^*} m_i \leq M_{j,k}^{\text{avail}}(t), \quad (12c)$$

#### IV. HYPERION: A TWO-STAGE HIERARCHICAL PARTITIONING AND SCHEDULING FRAMEWORK

As illustrated in Fig. 4, the Hyperion framework operates through a two-stage process to manage LLM inference across the network. The first stage is an offline, inter-tier partitioning phase where the central cloud strategically divides the LLM based on resource awareness of the multi-tier network. This partitioning results in a sequential deployment of the sub

models, creating a pipeline across the network tiers. The second stage consists of online, intra-tier task scheduling. Here, incoming prompts are tokenized and dispatched in real time, with the HypSched-RT algorithm dynamically mapping inference tasks to the optimal nodes within each tier for execution, from activation input to output forwarding. This scheduling process selects a single, most suitable device from each tier's node cluster to handle its portion of the inference task.

##### A. Stage 1: Offline inter-tier LLM Partitioning via HypSplit-DP

Here we aim to determine the optimal model partition vector  $\mathbf{p}^* = (p_1^*, p_2^*, \dots, p_{T-1}^*)$ , which can be expressed as  $\mathcal{P}_1$ . For notational convenience, we define the computing load of the  $j$ -th tier as  $L_j(\mathbf{p}) = \frac{1}{C_j} \sum_{i=p_{j-1}+1}^{p_j} f_i$ , where  $p_0 = 0$  and  $p_T = N$ . Therefore, the objective function can be concisely expressed as  $\min_{\mathbf{p}} \max_{j \in \mathcal{T}} \{L_j(\mathbf{p})\}$ . It is noteworthy that the volume of data transmitted between adjacent tiers is  $\text{batch\_size} \times \text{sequence\_length} \times \text{hidden\_dim}$ , which is a constant value independent of the partitioning strategy  $\mathbf{p}$ . Consequently, the total inter-tier transmission time, represented by  $\sum_{j=1}^{T-1} \tau_{j,j+1}$ , can be disregarded during the optimization process as it does not affect the determination of the optimal solution.

This problem is formulated as a Min-Max combinatorial optimization problem. A brute force approach of enumerating all possible combinations of partitioning points, denoted by  $p$ , would lead to a combinatorial explosion. To address this, we have designed an algorithm that named Hyperion Split with Dynamic Programming, which we refer to as HypSplit-DP.

We transform the original problem into a decision problem: given a target maximum latency  $\tau$ , does a valid partitioning scheme  $p$  exist such that the computing latency of every tier does not exceed  $\tau$ . Specifically, we need to determine if there

exists a partitioning vector  $p = (p_1, \dots, p_{T-1})$  that satisfies the constraints of  $\mathcal{P}_1$  while also fulfilling the condition:

$$L_j(p) = \frac{\sum_{i=p_{j-1}+1}^{p_j} f_i}{C_j} \leq \tau, \quad \forall j \in \mathcal{T}. \quad (13)$$

Solving this efficiently allows us to then perform a binary search for  $\tau$  to find its minimum possible value, which corresponds to the optimal solution of the original problem. We employ dynamic programming to solve the decision subproblem  $P_{\text{check}}(\tau)$ . We define a boolean state variable,  $DP(j, n)$ , which is true if and only if there exists a feasible assignment of the first  $n$  decoder blocks ( $B_1, \dots, B_n$ ) to the first  $j$  computing tiers (Tier 1, ..., Tier  $j$ ) that satisfies both the latency and memory constraints.

**Definition 1.** The state  $DP(j, n)$  is true if and only if there exists a partition point  $k$  (where  $j-1 \leq k < n$ ) such that the following two conditions are satisfied:

- The first  $k$  modules can be feasibly partitioned among the first  $j-1$  tiers; that is,  $DP(j-1, k)$  is true.
- The modules from  $k+1$  to  $n$  are assigned as a single group to the  $j$ -th tier, and this assignment satisfies the latency and memory constraints of the given decision problem.

This logical relationship can be described by the following state transition:

$$DP(j, n) = \bigvee_{k=j-1}^{n-1} \left( DP(j-1, k) \wedge \left[ \frac{1}{C_j} \sum_{i=k+1}^n f_i \leq \tau \right] \wedge \left[ \sum_{i=k+1}^n m_i \leq M_j \right] \right), \quad (14)$$

in which  $\vee$  denotes the logical OR operation,  $\wedge$  denotes the logical AND operation, and  $[ \cdot ]$  is the Iverson bracket, which evaluates to 1 if the condition inside is true, and 0 otherwise. To improve computing efficiency, we pre calculate the prefix sums of  $f_i$  and  $m_i$ :

$$S_f(n) = \sum_{i=1}^n f_i, \quad (15)$$

$$S_m(n) = \sum_{i=1}^n m_i. \quad (16)$$

Hence, the interval sums can be computed efficiently:  $\sum_{i=k+1}^n f_i = S_f(n) - S_f(k)$  and  $\sum_{i=k+1}^n m_i = S_m(n) - S_m(k)$ . For the base case, at the first tier ( $j = 1$ ), the state  $DP(1, n)$  is true if and only if placing all of the first  $n$  modules on the first tier satisfies the constraints.

$$DP(1, n) = \left[ \frac{S_f(n)}{C_1} \leq \tau \right] \wedge [S_m(n) \leq M_1]. \quad (17)$$

The solution to the entire decision problem  $P_{\text{check}}(\tau)$  is determined by the value of  $DP(T, N)$ . If  $DP(T, N)$  is true,

---

**Algorithm 1** HypSplit-DP for Optimal Inter-tier Model Partitioning

---

```

1: Input: Number of blocks  $N$ , tiers  $T$ , block costs  $\{f_i\}, \{m_i\}$ , tier properties  $\{C_j\}, \{M_j\}$ , and precision  $\epsilon$ .
2: Output: Optimal partition vector  $\mathbf{p}^*$  and minimized maximum latency  $\tau^*$ .
3: Compute prefix sums:  $S_f[n] \leftarrow \sum_{i=1}^n f_i$  and  $S_m[n] \leftarrow \sum_{i=1}^n m_i$ .
4: Initialize binary search bounds  $\tau_{\text{low}}$  and  $\tau_{\text{high}}$ .
5: Initialize  $\mathbf{p}^* \leftarrow \text{null}$ ,  $\tau^* \leftarrow \tau_{\text{high}}$ .
6: while  $(\tau_{\text{high}} - \tau_{\text{low}}) > \epsilon$  do
7:   Set current target latency  $\tau_{\text{mid}} \leftarrow (\tau_{\text{low}} + \tau_{\text{high}})/2$ .
8:   Initialize DP table  $DP[j][n]$  to false and predecessor table  $P[j][n]$ .
9:   Set  $DP[0][0] \leftarrow \text{true}$ .
10:  for  $j \leftarrow 1$  to  $T$  do
11:    for  $n \leftarrow j$  to  $N$  do
12:      for  $k \leftarrow j-1$  to  $n-1$  do
13:        if  $DP[j-1][k]$  is true then
14:          Calculate computing load  $L_j \leftarrow (S_f[n] - S_f[k])/C_j$ .
15:          Calculate memory usage  $U_j \leftarrow S_m[n] - S_m[k]$ .
16:          if  $L_j \leq \tau_{\text{mid}}$  and  $U_j \leq M_j$  then
17:            Set  $DP[j][n] \leftarrow \text{true}$ .
18:            Record predecessor  $P[j][n] \leftarrow k$ .
19:            Break.
20:          end if
21:        end if
22:      end for
23:    end for
24:  end for
25:  if  $DP[T][N]$  is true then
26:    A feasible partition found, update optimal latency  $\tau^* \leftarrow \tau_{\text{mid}}$ .
27:    Adjust search upper bound  $\tau_{\text{high}} \leftarrow \tau_{\text{mid}}$ .
28:    Reconstruct partition vector  $\mathbf{p}^*$  by backtracking through  $P$ .
29:  else
30:    No feasible partition found, adjust search lower bound  $\tau_{\text{low}} \leftarrow \tau_{\text{mid}}$ .
31:  end if
32: end while
33: Return  $\mathbf{p}^*$  and  $\tau^*$ .

```

---

it indicates that a feasible scheme exists with a latency not exceeding  $\tau$ ; otherwise, no such scheme exists.

As illustrated in Algorithm 1, we first determine the initial lower and upper bounds of the latency,  $\tau_{\text{low}}$  and  $\tau_{\text{high}}$ . In each iteration, we select a midpoint value  $\tau_{\text{mid}}$  and solve a feasibility subproblem,  $P_{\text{check}}(\tau_{\text{mid}})$ , to ascertain whether the latency  $\tau_{\text{mid}}$  is achievable. This feasibility subproblem is efficiently solved using dynamic programming (DP). Specifically, we construct a DP table where the state  $DP(j, n)$  represents the feasibility

of partitioning the first  $n$  tasks among the first  $j$  nodes.

Based on the final state of the DP table,  $DP(T, N)$ , we adjust the boundaries for the binary search. If the state is true, it implies that a better solution may exist; thus, we update the upper bound to  $\tau_{\text{high}} = \tau_{\text{mid}}$  and record the currently feasible partitioning scheme. If it is false, it indicates that the current latency is too stringent and must be relaxed, so we update the lower bound to  $\tau_{\text{low}} = \tau_{\text{mid}}$ . This process iterates until the search interval is smaller than a predefined precision threshold  $\epsilon$ . Finally, the algorithm converges to the optimal objective value,  $\tau_{\text{high}}$ , and the optimal task partitioning vector,  $p^*$ , is retrieved by backtracking through the last successful DP table. The overall complexity of this algorithm is  $O(T \cdot N^2 \cdot \log(\frac{\tau_{\text{high}} - \tau_{\text{low}}}{\epsilon}))$ , which demonstrates excellent computing efficiency for practical problem sizes.

The HypSplit-DP algorithm guarantees convergence to the optimal solution of subproblem  $\mathcal{P}_1$ . It exploits the problem's monotonicity, that is, a feasible maximum delay  $\tau$  implies any  $\tau' > \tau$  is also feasible. In each search iteration, a DP check,  $P_{\text{check}}(\tau)$ , serves as an exhaustive feasibility checker. Its state  $DP(j, n)$  and transition function systematically exhaust all valid combinations for partitioning  $N$  blocks into  $T$  tiers by iterating through all possible preceding split points  $k$ .

### B. Stage 2: Online intra-tier Task Scheduling via HypSched-RT

Once the optimal model partition  $p^*$  is determined, the task assigned to tier  $j$  becomes fixed, with a total computing workload of  $F_j^* = \sum_{i=p_{j-1}^*+1}^{p_j^*} f_i$ . When an inference task arrives at tier  $j$  at time  $t$ , the scheduler must select a node  $k$  from the set of nodes at that tier,  $\mathcal{K}_j$ , to execute the task. This selection process constitutes the scheduling problem,  $\mathcal{P}_{\text{sched}}$ . We reformulate the P2 problem as follows:

$$k^* = \arg \min_{k \in \mathcal{K}_j} \left( T_{j,k}^{\text{wait}}(t) + \frac{\sum_{i=p_{j-1}^*+1}^{p_j^*} f_i}{C_{j,k}} \right), \quad (18a)$$

$$\text{s.t. Node } k \text{ is available at time } t, \quad (18b)$$

$$\sum_{i=p_{j-1}^*+1}^{p_j^*} m_i \leq M_{j,k}^{\text{avail}}(t), \quad (18c)$$

We propose the Hyperion Scheduling for Real-Time (HypSched-RT) algorithm to handle the online challenge of arriving inference tasks. HypSched-RT enables intra-tier task parallelism by scheduling inference tasks across a tier's nodes ( $\mathcal{K}_j$ ). We maintain a task queue  $Q_{j,k}$ , for each node  $(j, k)$ , which enables the estimation of the waiting time  $T_{j,k}^{\text{wait}}(t)$ . The task queue  $Q_{j,k}$  is essential because individual edge nodes, such as the Jetson, possess limited parallel inference capabilities. When a new task arrives, we assume it is placed at the end of this queue, following a First In First Out (FIFO) strategy. At a given time  $t$ , the expected waiting time for node  $(j, k)$  is the sum of the remaining processing times for all tasks currently executing and those waiting in its queue. Let  $q_{j,k}^{\text{run}}(t)$  be the task being executed on node  $(j, k)$  at time  $t$ , and let  $Q_{j,k}^{\text{wait}}(t)$  be the set of tasks waiting in the queue of node  $(j, k)$ .

---

### Algorithm 2 HypSched-RT for Intra-tier Scheduling

---

```

1: Input: A new task with workload  $F_j^*$ ; the set of nodes  $K_j$  in tier  $j$ ; the real time state for each node  $k \in K_j$  (including  $C_{j,k}$ ,  $M_{j,k}^{\text{avail}}(t)$ ,  $F_{q_{j,k}^{\text{run}}(t),\text{rem}}(t)$ , and  $Q_{j,k}^{\text{wait}}(t)$ ); required memory  $m^{\text{act}}$ .
2: Output: The optimal node for execution,  $k^*$ .
3: Initialize minimum completion cost  $\text{min\_cost} \leftarrow \infty$ , and optimal node  $k^* \leftarrow \text{null}$ .
4: for each node  $k \in K_j$  do
5:   if node  $k$  is available and satisfies memory constraint  $M_{j,k}^{\text{avail}}(t) \geq m^{\text{act}}$  then
6:     Calculate the total workload of tasks already in its queue:  $F_{k,\text{queued}} \leftarrow F_{q_{j,k}^{\text{run}}(t),\text{rem}}(t) + \sum_{q' \in Q_{j,k}^{\text{wait}}(t)} F_{q'}$ .
7:     Compute the completion cost for the new task on node  $k$ :  $\text{cost}_k \leftarrow (F_{k,\text{queued}} + F_j^*)/C_{j,k}$ .
8:     if  $\text{cost}_k < \text{min\_cost}$  then
9:       Update the minimum cost:  $\text{min\_cost} \leftarrow \text{cost}_k$ .
10:      Designate node  $k$  as the current optimal node:  $k^* \leftarrow k$ .
11:    end if
12:  end if
13: end for
14: Return the determined optimal node  $k^*$ .

```

---

at time  $t$ . Let  $F_q$  denote the total computing workload of a task  $q$ , and let  $F_{q,\text{rem}}(t)$  be the remaining computing workload of task  $q$  at time  $t$ . The expected waiting time can be calculated as:

$$T_{j,k}^{\text{wait}}(t) = \frac{F_{q_{j,k}^{\text{run}}(t),\text{rem}}(t) + \sum_{q' \in Q_{j,k}^{\text{wait}}(t)} F_{q'}}{C_{j,k}}. \quad (19)$$

If no task is currently being executed, then  $F_{q_{j,k}^{\text{run}}(t),\text{rem}}(t) = 0$ . For a new task with a computing workload of  $F_j^*$  arriving at tier  $j$  at time  $t$ , the optimal scheduling decision  $k^*$  is to select the node that yields the earliest completion time. The completion time of the task on node  $k$ , denoted as  $T_{\text{complete}}(j, k, t)$ , is:

$$T_{\text{complete}}(j, k, t) = t + T_{j,k}^{\text{wait}}(t) + \frac{F_j^*}{C_{j,k}}. \quad (20)$$

Given that the current time  $t$  is a constant. Let  $\mathcal{K}_j^{\text{avail}}(t)$  denote the set of all nodes in tier  $j$  that satisfy the availability and real time memory constraints at time  $t$ . The optimal scheduling decision,  $k^*$ , is given by:

$$k^* = \arg \min_{k \in \mathcal{K}_j^{\text{avail}}(t)} \left\{ \frac{F_{q_{j,k}^{\text{run}}(t),\text{rem}}(t) + \sum_{q' \in Q_{j,k}^{\text{wait}}(t)} F_{q'}}{C_{j,k}} + \frac{F_j^*}{C_{j,k}} \right\}. \quad (21)$$

As illustrated in Algorithm 2, when a task arrives at any tier  $j$  of the network at time  $t$ , the scheduler immediately gathers real time status from all nodes  $k \in K_j$  within that tier. This information includes each node's available memory,

TABLE I: Specifications of the Multi-tier Network and LLM Architectures

Hardware Specifications				
Tier	Device	Qty.	TOPS	Mem (GB)
Tier 1	J. Orin Nano	3	67	8
Tier 2	J. Orin NX	3	157	16
Tier 3	J. AGX Orin	2	200	32
Model Architectures				
Model	Params	Blocks	Hid. Dim.	Attention
Llama3 8B	8B	32	4096	GQA
Phi-3-medium	14B	40	5120	GQA

$M_{j,k}^{\text{avail}}(t)$ , and the current load of its task queue, encompassing the remaining workload of the running task,  $F_{q_{j,k}}^{\text{run}}(t)$ ,  $\text{rem}(t)$ , and the tasks in its waiting queue,  $Q_{j,k}^{\text{wait}}(t)$ . Subsequently, the algorithm filters these nodes based on availability and memory constraints to establish a set of candidate nodes,  $K_j^{\text{avail}}(t)$ . Finally, by calculating the expected completion time for the task on each candidate node  $k$  as  $T_{\text{complete}}(j, k, t) = t + T_{j,k}^{\text{wait}}(t) + F_j^*/C_{j,k}$ , the scheduler assigns the task to the node  $k^*$  that offers the minimum expected completion time. The HypSched-RT algorithm is lightweight by design, achieving an optimal computational complexity upper bound of  $O(K_j)$ . This efficiency stems from its deterministic, single-pass linear scan, which eschews complex search-based heuristics. As detailed in Algorithm 2, the scheduler iterates through the  $K_j$  nodes exactly once. Within this pass, it executes only constant-time operations (e.g., status checks) for each node. This direct approach ensures rapid, real-time decision-making with negligible computation overhead.

## V. EXPERIMENT AND MODEL EVALUATION

### A. Experimental Setup and Baselines

To evaluate the performance of the Hyperion framework, we designed the following network. The setup comprised three computing tiers, each consisting of multiple heterogeneous NVIDIA Jetson nodes. Following the pipeline parallelism model, the inference tasks flow sequentially from Tier 1 to Tier 3. For clarity, the heterogeneity considered in our study is across tiers: within each tier, all nodes are of the same device model. The specific configurations for each tier, including the device type, quantity, computing, and memory, are detailed in Table I. To evaluate the generality of our scheduling framework, we also evaluate Hyperion on the Llama3 8B and Phi-3-medium models, with their architectural differences detailed in Table I. The input size for all tasks was standardized to 64 tokens, and the generation length was set to 128 tokens for each task.

To evaluate the system under a dynamic workload, we model the arrival of inference tasks as a Poisson process with an average arrival rate of  $\lambda = 0.2$  tasks per second [47]. We used the Linux TC traffic control tool to emulate communication bandwidths of 1 Gbps and 100 Mbps. For the offline model partitioning stage, the precision threshold for the HypSplit-DP algorithm's binary search is set to  $\epsilon = 10^{-3}$ , ensuring millisecond level accuracy in latency optimization. To benchmark the performance of the Hyperion algorithm, comparisons were drawn against following baselines.

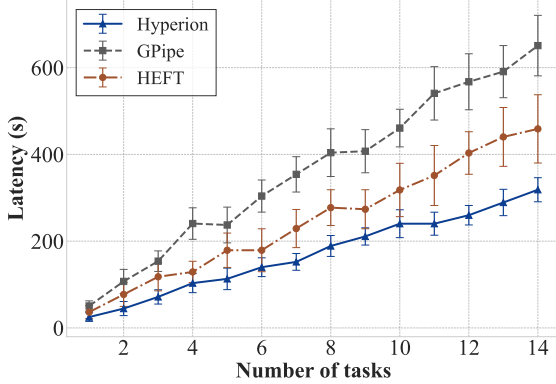
- **Heterogeneous Earliest Finish Time (HEFT):** To provide a robust heuristic based benchmark, we implement the HEFT algorithm. This approach first employs a memory aware greedy strategy to partition the LLM into contiguous blocks and assign them to different computing tiers [48]. Subsequently, for intra-tier scheduling, the classic HEFT algorithm prioritizes tasks based on their upward rank and maps each task to the node offering the earliest finish time.
- **GPipe style Partitioning with GNN based Scheduling (GPipe):** To benchmark against a modern learning based method, we developed a second baseline. For inter-tier partitioning, it adopts the classic static, load balanced partitioning strategy of the GPipe framework, which divides the model into contiguous segments [33]. For intra-tier scheduling, it then leverages a Graph Neural Network (GNN) to generate an optimal policy for mapping the assigned model segments to specific nodes [17].
- **Hierarchical resource aware Scheduling for Parallel LLM Inference (Hyperion):** Central to this study, Hyperion optimizes LLM inference in multi-tier networks through a two-stage scheduling framework. Hyperion first performs offline model partitioning using the HypSplit-DP algorithm, followed by online, real time task scheduling with the HypSched-RT algorithm.

### B. Comparative Analysis of end-to-end Latency

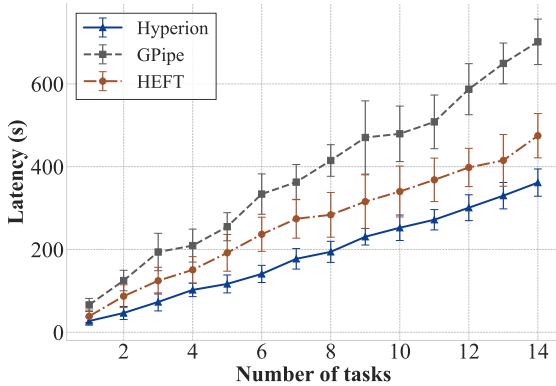
We conducted experiments within the three tier architecture, and the results are shown in Fig. 5. Using the LLaMA3 model, we tested at bandwidths of 1 Gbps, as presented in Fig. 5(a). The x axis represents the number of tasks from 1 to 14, while the y axis shows the average latency required to complete these tasks. The performance of GPipe, HEFT, and Hyperion are represented by the grey dashed line, brown dash dotted line, and blue solid line, respectively. Clearly, the latency of GPipe and HEFT is significantly higher than that of Hyperion, with GPipe consistently showing the highest latency. Specifically, when the task count reaches 14, GPipe and HEFT take approximately 637s and 451s, respectively, while Hyperion takes about 312s. At this point, the latency for GPipe and HEFT are 51.0% and 30.8% higher than Hyperion's, respectively. This demonstrates that Hyperion effectively implements model partitioning and scheduling, showing its efficiency in the multi-tier network.

In Fig. 5(b), we tested at bandwidths of 100 Mbps. As the number of tasks increased from 1 to 14, the latency for GPipe and HEFT increased from approximately 52.7s to 641.5s and from 38.5s to 471.1s, respectively. This shows total latency increases of 588.8s for GPipe and 432.6s for HEFT. In contrast, Hyperion's latency increased from about 27.5s to 368.8s, a more modest increase of only 341.3s. This represents a reduction in latency growth of 42.0% compared to GPipe and 21.1% compared to HEFT. This indicates that when the task number surges, Hyperion can optimize task distribution across tiers via its model partitioning algorithm, thereby utilizing resources more efficiently and reducing task latency.

To further validate the performance of Hyperion under different models, we replaced the larger Phi-3-medium model



(a) 1 Gbps

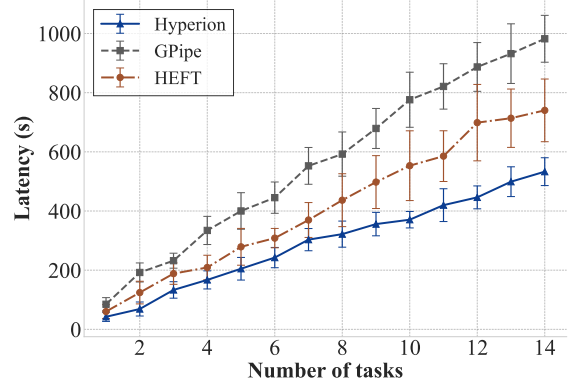


(b) 100 Mbps

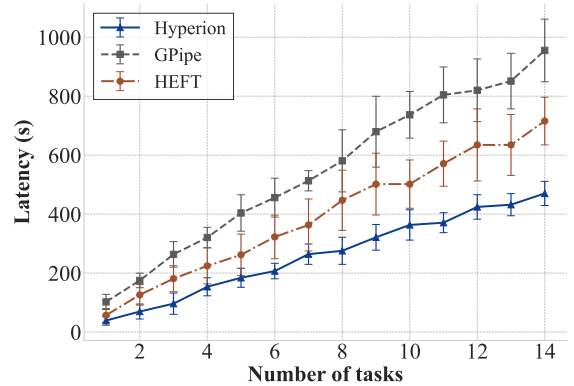
Fig. 5: Comparative Analysis of end-to-end Latency for Hyperion using the Llama 3 Model under Increasing Task Loads at (a) 1 Gbps and (b) 100 Mbps Bandwidths.

for testing. In Fig. 6(a), the curve corresponding to Hyperion still remains at the bottom, indicating the shortest latency across all task counts. The latency for GPipe and HEFT are both significantly higher than that of Hyperion, with GPipe consistently demonstrating the highest latency. For example, when the number of tasks reaches 10, the latency for Hyperion is approximately 355s, whereas HEFT and GPipe require about 516s and 742s, respectively. At this point, the latency for HEFT is approximately 31.2% higher than Hyperion, while GPipe's latency is 52.1% higher. This suggests that for the new Phi-3 model, Hyperion still achieves the lowest latency through superior model scheduling, outperforming the other algorithms. When the bandwidth decreases from 1Gbps to 100Mbps, the results shown in Fig. 6(b). Hyperion demonstrated a clear advantage in both latency and the rate of increase in reference time as task grew. The first two sets of experiments shown that, the efficient scheduling of Hyperion enables faster completion of inference under various model and bandwidth.

Table II presents a performance of Hyperion with the Llama3 and Phi-3 models on three-tier network in more detail. Our analysis reveals several key findings. First, the Phi-3-medium model is demonstrably more resource intensive than Llama3 8B, exhibiting higher end-to-end latency and consum-



(a) 1 Gbps



(b) 100 Mbps

Fig. 6: Comparative Analysis of end-to-end Latency for Hyperion using the Phi-3-medium Model under Increasing Task Loads at (a) 1 Gbps and (b) 100 Mbps Bandwidths.

ing more GPU and memory resources across all configurations. For instance, under the 1 Gbps condition, Phi-3-medium's latency was 35.9% higher than Llama3's (38.7s vs. 24.8s), with its memory utilization on the AGX Orin being notably higher (69.2% vs. 42.7%).

Second, a clear trend is observed regarding device capability: as computing decreases from the AGX Orin to the Orin Nano, both average GPU and memory utilization consistently increase for any given model and bandwidth. This indicates that less powerful devices must operate at a higher capacity to handle the workload. For example, with Llama3 at 1 Gbps, GPU utilization rises from 45.9% on AGX Orin to 52.1% on Orin Nano. Finally, network bandwidth has a direct impact on performance. Reducing the bandwidth from 1 Gbps to 100 Mbps increased end-to-end latency by 9.7% for Llama3 and 8.5% for Phi-3-medium. Interestingly, the number of allocated blocks for each device remained constant regardless of bandwidth, suggesting a static allocation strategy, whereas performance metrics like latency and GPU utilization are dynamically affected by network conditions.

### C. Resource Utilization Efficiency

We evaluated the GPU utilization of three algorithms, exemplified on the AGX Orin nodes. With results illustrated

TABLE II: Performance Breakdown of the Hyperion Framework: A Detailed Look at Latency, Resource Utilization, and Block Allocation Across Tiers for Llama 3 and Phi-3 Models at Varied Bandwidths.

Model	Condition	Metric	Jetson Device		
			AGX Orin	Orin NX	Orin Nano
Llama3 8B	1 Gbps Bandwidth	Avg. GPU Util. (%)	45.9%	47.2%	52.1%
		Avg. Mem. Util. (%)	42.7%	45.2%	53.1%
		Alloc. Blocks	18	9	5
	100 Mbps Bandwidth	end-to-end Latency (s)	24.8		
		Avg. GPU Util. (%)	43.3%	45.3%	50.2%
		Avg. Mem. Util. (%)	42.7%	45.2%	53.2%
Phi-3-medium	1 Gbps Bandwidth	Alloc. Blocks	18	9	5
		end-to-end Latency (s)	27.2		
		Avg. GPU Util. (%)	53.6%	55.3%	59.3%
	100 Mbps Bandwidth	Avg. Mem. Util. (%)	69.2%	78.3%	83.1%
		Alloc. Blocks	20	13	7
		end-to-end Latency (s)	38.7		
	100 Mbps Bandwidth	Avg. GPU Util. (%)	49.7%	51.8%	55.7%
		Avg. Mem. Util. (%)	69.2%	78.4%	83.3%
		Alloc. Blocks	20	13	7
	end-to-end Latency (s)	42.0			

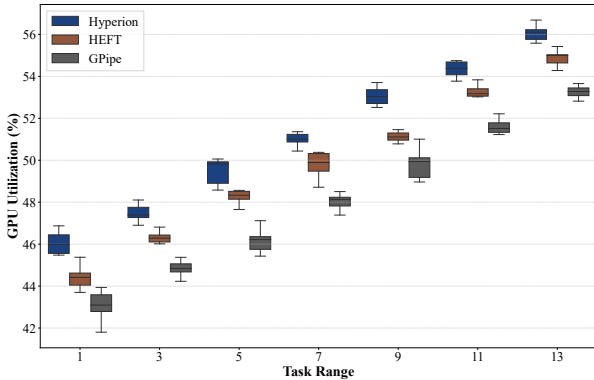


Fig. 7: GPU Utilization Efficiency on the AGX Orin: A Comparison of Hyperion, HEFT, and GPipe with Increasing Task Range.

in Fig. 7, at 3 tasks, Hyperion exhibited the highest median GPU utilization at approximately 47.4%. HEFT showed a slightly lower median usage of about 46.3%, while GPipe had the lowest at around 44.9%. When scaled to 13 tasks, all algorithms demonstrated elevated GPU utilization. Hyperion's median utilization rose to approximately 56.1%. At this point, the median GPU utilization of HEFT and GPipe also increased, to about 55.0% and 53.2% respectively, but remained lower than that of Hyperion. This means that by optimizing task scheduling in stage two, Hyperion achieves superior utilization of network resources, minimizing device idle time and reducing latency.

Next, we record the resource utilization of each tier device when running the LLama3. As shown in Fig. 8 (a), devices in Tier 1 demonstrated the most intensive resource usage, with GPU utilization clustered between approximately 51.2% and 53.5% and corresponding memory utilization ranging from 51.6% to 53.8%. Following this, Tier 2 nodes operated at

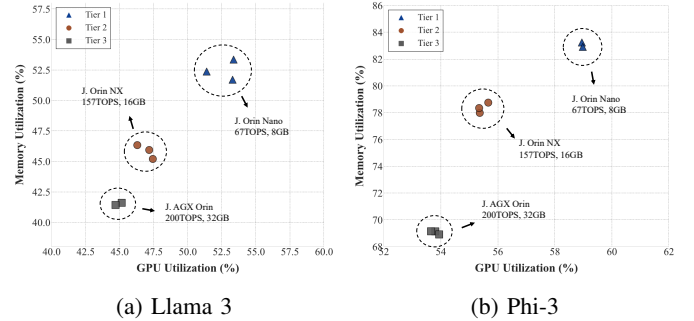
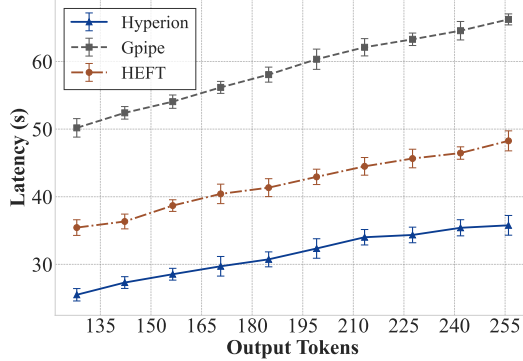


Fig. 8: Tier Wise Resource Utilization under the Hyperion Framework: A Scatter Plot Analysis of GPU vs. Memory Consumption for (a) Llama 3 and (b) Phi-3 Models.

an intermediate level, exhibiting GPU utilization in the range of 46.1% to 47.5% and memory utilization between 45.1% and 46.5%. Tier 3 nodes showed the lowest consumption, with GPU utilization around 45% and memory utilization consistently around 42%.

Analysis of the Phi model's tier wise resource utilization also reveals a clear hierarchical structure in Fig. 8 (b). GPU utilization was distinctly stratified, with Tier 1 averaging approximately 59.0%, followed by Tier 2 at 55.3-56.0% and Tier 3 at 53.5-54.0%. This hierarchical pattern was even more pronounced in memory consumption, where Tier 1 reached roughly 83.0%, Tier 2 clustered around 78.0-79.0%, and Tier 3 used the least at approximately 69.0%. This confirms that the resource utilization of nodes within each tier remained stable, indicating that Hyperion achieves effective task scheduling. Furthermore, devices at lower tiers exhibited higher resource utilization, which can likely be attributed to their more limited resources. This observation also underscores the efficacy of the HypSplit-DP algorithm's load balancing strategy. By allocating a computing load to more capable higher tier devices,



(a) Llama 3

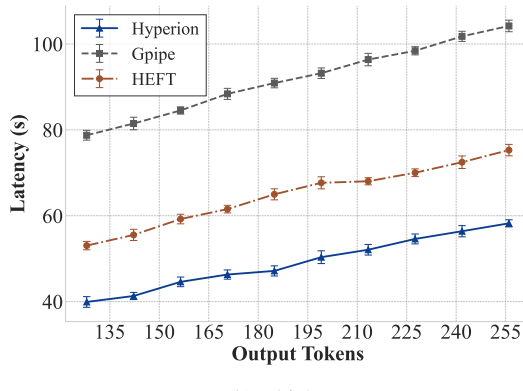


Fig. 9: end-to-end Latency Comparison of Hyperion, HEFT, and GPipe across Different Token Output for (a) Llama 3 and (b) Phi-3.

the framework successfully balances system wide throughput, compelling the less resourced devices to operate near their capacity to maintain pace.

#### D. Scalability with Increasing Output Tokens

Next, we tested the performance difference between Hyperion and the baseline algorithm under different output tokens. As shown in Fig. 9 (a), GPipe, consistently demonstrates the highest latency, starting at 50.1s for 128 tokens and rising steeply to about 66.2s at 256 tokens. The HEFT algorithm, performs slightly better but follows a similar steep trajectory, with its latency increasing from 35.0s to 48.1s over the same token range. In contrast, Hyperion proves to be the most efficient algorithm. It begins with the lowest latency of approximately 25.2s at 128 tokens and concludes at a significantly lower 35.8s at 256 tokens.

Next we tested Hyperion’s performance on the Phi in Fig. 9 (b), which reveals a widening performance gap as output tokens increase. While the initial latencies at 128 tokens were closely clustered between 40.1s (Hyperion), 53.4s (HEFT) and 78.7s (GPipe), their different scaling efficiencies led to a significant divergence. By the 256 token, Hyperion’s latency reached only 57.6s, whereas HEFT and GPipe climbed to 74.5s and 103.7s, respectively. This demonstrates Hyperion’s

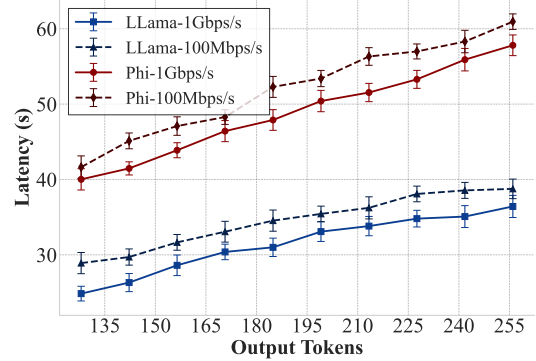
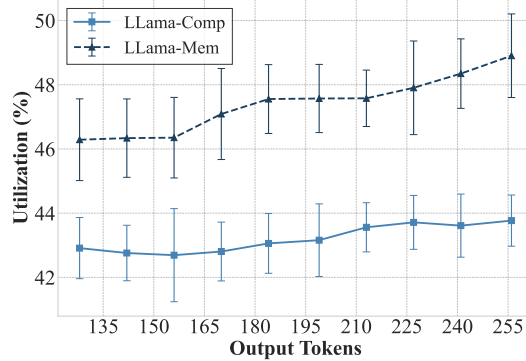


Fig. 10: Impact of Bandwidth Variation on the Performance of the Hyperion across Different Output Token.

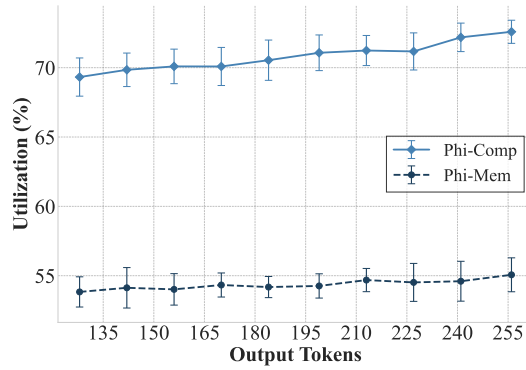
superior scalability, making its end-to-end latency approximately 22.7% lower than HEFT’s and 44.5% lower than GPipe’s for longer generative tasks. The consistent outperformance of Hyperion over HEFT and GPipe, suggesting that its resource aware mechanism prevents the creation of “bottleneck” nodes in stage one, thereby optimizing overall latency.

Fig. 10 shows the performance of Hyperion under different models and bandwidths. As shown in the figure, there is an positive correlation between latency and the number of tokens. Specifically, under a 1Gbps bandwidth condition (solid line), its latency for Phi-3 grows from approximately 40.1s at 128 tokens to 57.6s at 256 tokens. The 100Mbps condition (dashed line) for Phi-3 follows a nearly identical trajectory, starting slightly higher at 41.8s and reaching 60.8s. In stark contrast, the Llama 3 model, represented by lines with blue, demonstrates substantially lower latency. For the 1Gbps case (solid line), Llama 3’s latency increases only modestly from 25.2s to 36.1s across the same token range. The performance at 100Mbps (dashed line) is almost indistinguishable, rising from 28.4s to 38.3s. Overall, Fig. 10 indicates that the latency of Phi-3 is more sensitive to the output length, suggesting inferior performance scalability. In contrast, Llama 3 exhibits a more flat latency growth curve, demonstrating its stability in generating long texts. Also, the system’s performance bottleneck is compute bound rather than constrained by network bandwidth. Despite a tenfold difference in bandwidth, the impact on total latency is negligible, typically resulting in a disparity of only 2-3 seconds.

The resource utilization on the AGX Orin under the Hyperion was statistically analyzed. It was observed that computing and memory resources exhibit divergent trends as the number of output tokens increases. As shown in Fig. 11 (a), the computing utilization, represented by a solid line with light blue, exhibits a positive and linear correlation with the token count. It begins at approximately 42.9% utilization for 128 tokens and steadily climbs to a peak of around 48.8% at 256 tokens, clearly indicating that the computing load scales directly with the length of the generation tokens. In contrast, the memory utilization, depicted by a dashed line with dark blue, remains almost entirely static across the entire observed



(a) Llama 3



(b) Phi-3

Fig. 11: Analysis of Llama 3 and Phi-3’s Resource Utilization on AGX Orin with Increasing Token.

range. It maintains a constant utilization level of approximately 43%, irrespective of the number of tokens being generated.

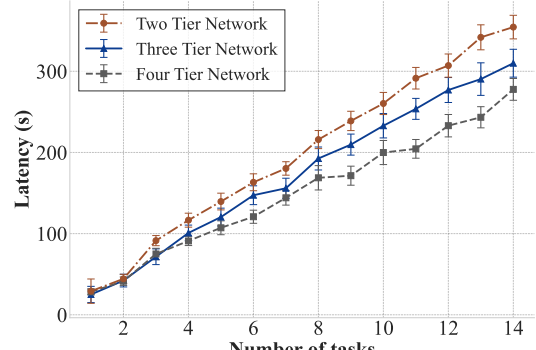
Next we use the larger Phi-3 for statistics shown in Fig. 11 (b). Memory utilization, demonstrates remarkable stability across the entire token generation process. It hovering in a narrow band between approximately 54% and 55%. In contrast, the computing load, is both significantly higher and more dynamic, exhibiting a gentle upward trend. Starting from an already high utilization of around 69.0% at 128 tokens, it fluctuates as the token count increases, eventually reaching its peak of approximately 72.6% at 256 tokens. This opposing behavior in two models suggests that while the computing demand is dynamic and dependent on the workload, the memory footprint is largely fixed once the model is loaded for inference. This points to a stable memory allocation for the model’s weights and associated caches during the generation process.

#### E. Performance across Different Network Architectures

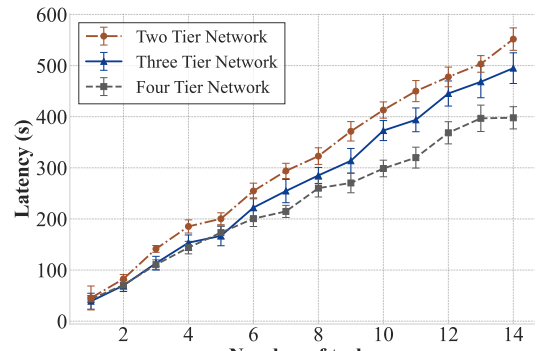
Next, we evaluate the performance of Hyperion on different network topologies. The network configuration for each case is shown in Table III. The network structure becomes progressively more complex, with the number of layers increasing from two to four, and the total amount of resources gradually expands. It is important to note that within each network, nodes at lower layers have weaker capabilities.

TABLE III: Definition of Heterogeneous Network Topologies for Scalability Evaluation.

Network Config.	Tier	Device	Quantity
Two-Tier	Tier 1	J. Orin NX	3
	Tier 2	J. AGX Orin	2
Three-Tier	Tier 1	J. Orin Nano	3
	Tier 2	J. Orin NX	3
	Tier 3	J. AGX Orin	2
Four-Tier	Tier 1	J. Orin Nano	2
	Tier 2	J. Orin Nano	2
	Tier 3	J. Orin NX	3
	Tier 4	J. AGX Orin	3



(a) Llama 3



(b) Phi-3

Fig. 12: Performance of Hyperion for Llama 3 and Phi-3 Deployment Across Various Network Architectures.

Fig. 12 (a) illustrates the average latency across different network architectures as a function of the number of tasks. The x axis represents the number of tasks, and the y axis represents the latency in seconds. The figure presents three latency curves: the two tier network (dash dot brown line), the three tier network (solid blue line), and the four tier network (dashed grey line). At 6 tasks, the latencies for the four tier, three tier, and two tier networks were approximately 138.3s, 146.1s, and 164.0s, respectively. As the number of tasks increased to 14, the four tier network’s latency reached approximately 261.5s, while the three tier and two tier networks experienced higher latencies of approximately 303.8s and 347.8s, respectively. This indicates that the three tier and two tier networks exhibited latencies approximately 16.2% and 33.0% higher than the four tier network, respectively.

We then deployed the larger Phi-3 in the Hyperion framework. A clear trend in Fig. 12 (b) of performance divergence is evident as the task load intensifies. Initially, under a light load of four tasks, the three tier and four tier networks demonstrate comparable latency at approximately 150.0s, while the two tier network lags slightly at around 178.2s. This disparity is further magnified at the maximum tested load of 14 tasks, where the latency for the two tier, three tier, and four tier systems reaches approximately 573.3, 501.5, and 427.2s, respectively. Fig. 12 reveals that the benefits of a multi-tier network architecture are significantly amplified when deploying larger, more computingly intensive models. While the four tier network is the optimal configuration for both models, the performance degradation in two and three tier systems is far more pronounced with the larger Phi-3 model.

## VI. CONCLUSION

This paper addressed the challenge of the end-to-end latency optimization for LLM inference within resource-constrained, heterogeneous multi-tier networks. We define this as a cross-tier resource orchestration problem, where device heterogeneity and strict memory/GPU limits are dominant, coupled constraints. To solve this, we pioneer Hyperion, a hierarchical framework. Implementing this dual-driven (model & task aware) optimization. It first determines a global aware, resource-balanced model partition via the offline HypSplit-DP algorithm. Subsequently, the lightweight, online HypSched-RT algorithm leverages this fixed partition to perform real-time, dynamic task dispatch, adapting instantly to device status to minimize queuing delays.

Our evaluation validates Hyperion's superiority, demonstrating performance gains over established baselines across multiple models and scenarios. For instance, with the Llama3 8B model under a heavy load of 14 tasks, Hyperion achieved an average latency of approximately 312s, outperforming HEFT by 31.2% and GPipe by 52.1%. The framework's scalability was particularly evident in long sequence generation tasks. Specifically, when generating 256 output tokens with the Phi-3 model, GPipe's latency of 103.7s was approximately 44.5% higher than Hyperion's 57.6s. Moreover, Hyperion's architecture inherently bolsters data security; by processing data locally at lower tiers, it minimizes network exposure and mitigates interception risks. These findings prove that a hierarchical, resource aware strategy is critical for the practical deployment of LLM at the network edge. This work, therefore, paves the way for more advanced, low latency services, with future research poised to explore additional optimizations such as energy efficiency.

## REFERENCES

- [1] A. Vaswani, et al., "Attention is All You Need," *Advances in Neural Information Processing Systems*, 2017.
- [2] Y. He, J. Fang, F. R. Yu, and V. C. Leung, "Large Language Models (LLMs) Inference Offloading and Resource Allocation in Cloud-Edge Computing: An Active Inference Approach," *IEEE Transactions on Mobile Computing*, vol. 23, no. 12, pp. 11253-11264, Dec. 2024.
- [3] IDC, "Worldwide Global DataSphere IoT Device and Data Forecast, 2021–2025," 2021.
- [4] W. Shi, et al., "Edge Computing: Vision and Challenges," *IEEE Internet of Things Journal*, vol. 3, no. 5, pp. 637-646, 2016.
- [5] J. Huang, et al., "Dynamic UAV-Assisted Cooperative Edge AI Inference," *IEEE Transactions on Wireless Communications*, vol. 24, no. 1, pp. 615-628, Jan. 2025.
- [6] X. Li and S. Bi, "Optimal AI Model Splitting and Resource Allocation for Device-Edge Co-Inference in Multi-User Wireless Sensing Systems," *IEEE Transactions on Wireless Communications*, vol. 23, no. 9, pp. 11094-11108, Sept. 2024.
- [7] NVIDIA, "Jetson Nano Developer Kit," 2019. [Online]. Available: <https://developer.nvidia.com/embedded/jetson-nanodeveloper-kit>.
- [8] N. Singh and M. Adhikari, "A Hybrid Semi-Asynchronous Federated Learning and Split Learning Strategy in Edge Networks," *IEEE Transactions on Network Science and Engineering*, vol. 12, no. 2, pp. 1429-1439, March-April 2025.
- [9] M. Ma, C. Gong, L. Zeng, Y. Yang and L. Wu, "FlocOff: Data Heterogeneity Resilient Federated Learning With Communication-Efficient Edge Offloading," in *IEEE Journal on Selected Areas in Communications*, vol. 42, no. 11, pp. 3262-3277, Nov. 2024.
- [10] Y. Yang, M. Ma, Y. Huang, H. Chai, C. Gong, H. Geng, Y. Zhou, et al., "Agentic Web: Weaving the Next Web With AI Agents," *arXiv preprint arXiv:2507.21206*, 2025.
- [11] Y. Yang, et al., "6G Network AI Architecture for Everyone-Centric Customized Services," *IEEE Network*, vol. 37, no. 5, pp. 71-80, Sept. 2023.
- [12] M. Ma, C. Gong, L. Zeng and Y. Yang, "MOGR: Multi-task Offloading via Graph Representation in Heterogeneous Computing Network," *ICC 2024 - IEEE International Conference on Communications*, Denver, CO, USA, 2024, pp. 1237-1242.
- [13] P. Mach and Z. Becvar, "Mobile Edge Computing: A Survey on Architecture and Computation Offloading," *IEEE Communications Surveys & Tutorials*, vol. 19, no. 3, pp. 1628-1656, 2017.
- [14] Y. Cheng, et al., "A Survey of Model Compression and Acceleration for Deep Neural Networks," *arXiv preprint arXiv:1710.09282*, 2017.
- [15] K. Liu, J. Wang, Z. Huang, and J. Pan, "Sampling-Based Multi-Job Placement for Heterogeneous Deep Learning Clusters," *IEEE Transactions on Parallel and Distributed Systems*, vol. 35, no. 6, pp. 1029-1043, June 2024.
- [16] Z. Zhang, Y. Zhao, H. Li, C. Lin, and J. Liu, "DVFO: Learning-Based DVFS for Energy-Efficient Edge-Cloud Collaborative Inference," *IEEE Transactions on Mobile Computing*, vol. 23, no. 10, pp. 9042-9059, Oct. 2024.
- [17] M. Ma, C. Gong, L. Zeng and Y. Yang, "multi-tier Multi-Node Scheduling of LLM for Collaborative AI Computing," *IEEE INFOCOM 2025 - IEEE Conference on Computer Communications*, London, United Kingdom, 2025, pp. 1-10.
- [18] X. Zhang, et al., "Beyond the Cloud: Edge Inference for Generative Large Language Models in Wireless Networks," *IEEE Transactions on Wireless Communications*, vol. 24, no. 1, pp. 643-658, Jan. 2025.
- [19] X. Xu, G. Feng, Y. Liu, S. Qin, J. Wang, and Y. Wang, "Joint Inference Offloading and Model Caching for Small and Large Language Model Collaboration," *IEEE Transactions on Mobile Computing*, 2025.
- [20] D. Xu, et al., "EdgeLLM: Fast On-Device LLM Inference With Speculative Decoding," *IEEE Transactions on Mobile Computing*, vol. 24, no. 4, pp. 3256-3273, April 2025.
- [21] S. Teerapittayanon, B. McDanel, and H. T. Kung, "Distributed Deep Neural Networks Over the Cloud, the Edge and End Devices," *Proceedings of the 2017 IEEE 37th International Conference on Distributed Computing Systems (ICDCS)*, 2017, pp. 328-339.
- [22] S. Teerapittayanon, B. McDanel, and H. T. Kung, "BranchyNet: Fast Inference via Early Exiting From Deep Neural Networks," *Proceedings of the 2016 23rd International Conference on Pattern Recognition (ICPR)*, 2016, pp. 2464-2469.
- [23] F. Dong et al., "Multi-Exit DNN Inference Acceleration Based on Multi-Dimensional Optimization for Edge Intelligence," *IEEE Transactions on Mobile Computing*, vol. 22, no. 9, pp. 5389-5405, 1 Sept. 2023.
- [24] S. Han, H. Mao, and W. J. Dally, "Deep Compression: Compressing Deep Neural Networks With Pruning, Trained Quantization and Huffman Coding," *Proceedings of the International Conference on Learning Representations (ICLR)*, 2016.
- [25] W. Li, et al., "MobileBERT: A Compact Task-Agnostic BERT for Resource-Limited Devices," *Proceedings of the Annual Meeting of the Association for computing Linguistics (ACL)*, 2020, pp. 2158-2170.
- [26] G. Hinton, O. Vinyals, and J. Dean, "Distilling the Knowledge in a Neural Network," *arXiv preprint arXiv:1503.02531*, 2015.
- [27] S. Kim, et al., "Sequence-Level Knowledge Distillation," *Proceedings of the Conference on Empirical Methods in Natural Language Processing (EMNLP)*, 2016, pp. 1317-1327.

- [28] S. Wang, et al., "Adaptive Federated Learning in Resource Constrained Edge Computing Systems," *IEEE Journal on Selected Areas in Communications*, vol. 37, no. 6, pp. 1205-1221, 2019.
- [29] L. Gu, D. Zeng, S. Guo, and A. Barnawi, "Cost Efficient Resource Management in Fog Computing Supported Medical Cyber-Physical System," *IEEE Transactions on Emerging Topics in Computing*, vol. 7, no. 2, pp. 131-143, 2018.
- [30] W. Lin, et al., "Task Offloading and Resource Allocation for Mobile Edge Computing With Deep Reinforcement Learning," *IEEE Transactions on Vehicular Technology*, vol. 69, no. 1, pp. 431-445, 2020.
- [31] Y. Xiao, et al., "Edge Computing Security: State of the Art and Challenges," *Proceedings of the IEEE*, vol. 107, no. 8, pp. 1608-1631, 2019.
- [32] Z. Zhou, et al., "Secure and Efficient Vehicle-to-Grid Energy Trading in Cyber Physical Systems: Integration of Blockchain and Edge Computing," *IEEE Transactions on Systems, Man, and Cybernetics: Systems*, vol. 50, no. 1, pp. 43-57, 2019.
- [33] Y. Huang, et al., "GPipe: Efficient Training of Giant Neural Networks Using Pipeline Parallelism," *Advances in Neural Information Processing Systems (NeurIPS)*, 2019, pp. 103-112.
- [34] N. Goyal, et al., "PipeDream: Generalized Pipeline Parallelism for DNN Training," *Proceedings of Machine Learning and Systems*, vol. 1, 2021, pp. 1-13.
- [35] M. Shoeybi, et al., "Megatron-LM: Training Multi-Billion Parameter Language Models Using Model Parallelism," *arXiv preprint arXiv:1909.08053*, 2019.
- [36] S. Laskaridis, et al., "SPINN: Synergistic Progressive Inference of Neural Networks Over Device and Cloud," *Proceedings of the 26th Annual International Conference on Mobile Computing and Networking*, 2020, pp. 1-15.
- [37] D. Narayanan, et al., "Memory-Efficient Pipeline-Parallel DNN Training," *arXiv preprint arXiv:2010.13038*, 2021.
- [38] R. Shi, et al., "Communication-Efficient Distributed Deep Learning With Merged Gradient Sparsification on GPUs," *IEEE Transactions on Parallel and Distributed Systems*, vol. 32, no. 5, pp. 1091-1104, 2021.
- [39] S. Zheng, et al., "Asynchronous Stochastic Gradient Descent With Delay Compensation," *Proceedings of the International Conference on Machine Learning (ICML)*, 2017, pp. 4120-4129.
- [40] Y. Li, et al., "Edge-Oriented Computing Paradigms: A Survey on Architecture Design and System Management," *ACM Computing Surveys*, vol. 51, no. 2, pp. 1-34, 2019.
- [41] Z. Zhou, et al., "Edge Intelligence: Paving the Last Mile of Artificial Intelligence With Edge Computing," *Proceedings of the IEEE*, vol. 107, no. 8, pp. 1738-1762, 2020.
- [42] S. Cen and Y. Zhu, "NP-LLM: A Unified Large-Language-Model-Assisted Framework of 6G Network-Layer Planning," *IEEE Communications Magazine*, vol. 63, no. 8, pp. 92-98, August 2025.
- [43] X. Wang, Y. Han, V. C. Leung, D. Niyato, X. Yan, and X. Chen, "Convergence of Edge Computing and Deep Learning: A Comprehensive Survey," *IEEE Communications Surveys & Tutorials*, vol. 22, no. 2, pp. 869-904, 2020.
- [44] Z. Wu, et al., "Recursive Offloading for LLM Serving in Multi-tier Networks," *arXiv preprint arXiv:2505.16502*, 2025.
- [45] P. Gupta and P. R. Kumar, "The capacity of wireless networks," *IEEE Transactions on Information Theory*, vol. 46, no. 2, pp. 388-404, Mar. 2002.
- [46] P. Belotti, et al., "Mixed-integer nonlinear optimization," *Acta Numerica*, vol. 22, pp. 1-131, 2013.
- [47] Y. Li, Z. Li, W. Yang, and C. Liu, "RT-LM: Uncertainty-Aware Resource Management for Real-Time Inference of Language Models," *arXiv preprint arXiv:2309.06619*, 2023.
- [48] H. Topcuoglu, S. Hariri, and M. Y. Wu, "Performance-Effective and Low-Complexity Task Scheduling for Heterogeneous Computing," *IEEE Transactions on Parallel and Distributed Systems*, vol. 13, no. 3, pp. 260-274, March 2002.